Pattern Recognition Letters 135 (2020) 57–63

Contents lists available at ScienceDirect

Pattern Recognition Letters

journal homepage: www.elsevier.com/locate/patrec

CNN-DMRI: A Convolutional Neural Network for Denoising of Magnetic Resonance Images☆

Prasun Chandra Tripathi*, Soumen Bag

Department of Computer Science and Engineering, Indian Institute of Technology (Indian School of Mines) Dhanabd, Dhanbad 826004, India

ARTICLE INFO

Article history:
Received 20 September 2019
Revised 26 December 2019
Accepted 31 March 2020
Available online 2 April 2020

Keywords:
Convolutional Neural Network
Denoising
Encoder-decoder
Magnetic Resonance Imaging
Residual learning

ABSTRACT

Magnetic Resonance Images (MRI) are often contaminated by rician noise at the acquisition time. This type of noise typically deteriorates the performance of disease diagnosis by a human observer or an automated system. Thus, it is necessary to remove the rician noise from MRI scans as a preprocessing step. In this letter, we propose a novel Convolutional Neural Network (CNN), viz. CNN-DMRI, for denoising of MRI scans. The network uses a set of convolutions to separate the image features from the noise. The network also employs encoder-decoder structure for preserving the prominent features of the image while ignoring unnecessary ones. The training of the network is carried out in an end-to-end way by utilizing residual learning scheme. The performance of the proposed CNN has been tested qualitatively and quantitatively on one simulated and four real MRI datasets. Extensive experimental findings suggest that the proposed network can denoise MRI images effectively without losing crucial image details.

© 2020 Elsevier B.V. All rights reserved.

1. Introduction

In current clinical practice, the role of medical images has become very prominent for the diagnosis and treatment of several diseases. The medical images are assisting the medical practitioners in the identification of a disease, locating the abnormal sites, monitoring tumor size, etc. Among different medical imaging modalities, Computer Tomography (CT), Magnetic Resonance Imaging (MRI), Positron Emission Tomography (PET), and Ultrasound are widely utilized by the physicians. MRI has particularly dominated its usage due to its effective soft tissue delineation with high spatial and temporal resolutions. Additionally, MRI scans are usually acquired in multiple channels (e.g., T1-w, T2-w, T1-C, FLAIR, etc.), which help the physician to precisely observe the internal soft tissues of the body. However, MRI scans are typically degraded by noise at the acquisition time due to imperfection in radio frequency coils or movement of the patient. Noise in MRI scans not only affects the performance of computerized diagnosis systems but also creates difficulty for the manual inspection of a disease. Due to this, denoising of MRI scans has a great significance in medical imaging, and it is considered as an active area of research [4].

Let $X \in \mathbb{R}^{P\times Q}$ is a true MRI, $Y \in \mathbb{R}^{P\times Q}$ is an observed MRI, and $N \in \mathbb{R}^{P\times Q}$ is noise. Thus, the observed image Y can be represented using the following equation.

$$Y = X + N \tag{1}$$

The MRI denoising methods try to reduce the noise N from the observed image Y, so that they can obtain an estimate $\hat{X}$ of true MRI X. The noise N in MRI images shows rician distribution [19] that has the Probability Density Function (PDF) p_M defined as follows.

$$p_M(M|X,\sigma_N) = \frac{M}{\sigma_N^2}\exp^{-\frac{(M^2+X^2)}{2\sigma_N^2}} J_0\left(\frac{XM}{\sigma_N^2}\right)h(M), \tag{2}$$

where $J_0(.)$ denotes zero order Bessel function, $h(.)$ represents Heaviside step function, X is a noise-free signal, σ_N^2 denotes noise variance, and M is a rician distributed random variable. The rician noise demonstrates signal dependent behavior in images that provides guassian distribution in high intensity pixels and rayleigh distribution in low intensity pixels. Because of this, MRI scans typically get low contrast, which creates the difficulty for MRI denoising techniques.

In the past, several research attempts have been devoted to enhance the quality of MRI images. These works can be broadly categorized into three groups, namely anisotropic diffusion based techniques [8,14,22], wavelet based techniques [1,2,24], and non-local means based techniques [3,6,17,18]. Anisotropic diffusion filter [8] removes the noise from the images by smoothing in lo-

☆ Editor: Prof. G. Sanniti di Baja.

* Corresponding author.
E-mail address: prasunchandratripathi@gmail.com (P.C. Tripathi).

https://doi.org/10.1016/j.patrec.2020.03.036
0167-8655/© 2020 Elsevier B.V. All rights reserved.

cal regions. This filter utilizes the edge-stopping function to avoid blurring of the edges. Tang et al. [22] have proposed an anisotropic diffusion filter that uses a novel gradient estimation method. In anisotropic diffusion filters, the estimation of noise plays a crucial role in denoising. Krissian and Aja-Fernández [14] have proposed a novel anisotropic diffusion filter which has an integrated noise estimation mechanism. The estimation of noise in wavelet domain [24] has been quite prevalent in image processing. Anand and Sahambi [1] have proposed a bilateral filter that works on undecimated wavelet transform domain for MRI denoising. Furthermore, Anand and Sahambi [2] have utilized neighbourhood similarity for preserving the edges of the images.

From the last decade, Non-Local Means (NLM) based filters [6,7,17,18] have been extensively utilized for MRI denoising. These filters [6] exploit redundant information present in the images for the denoising process. In fact, NLM based filters eliminate noise by taking average of non-local patches. Manjón et al. [17] have modified the basic NLM filter for removal of rician noise from MRI images. Furthermore, the authors [18] have proposed a two-stage NLM based MRI denoising method. This method firstly performs non-local PCA thresholding, and then it uses the rotationally invariant NLM filter for MRI denoising. Chen et al. [7] have presented an NLM based filter which collaboratively denoises MRI images. The majority of the aforementioned methods are time-consuming as they need some form of optimization [9]. Moreover, the performance of such traditional methods typically depends on the tuning of some parameters.

Recently, Convolution Neural Networks (CNNs) have obtained remarkable performances on several low-level image processing tasks such as image super resolution [15], image denoising [23,25,26], image dehazing [23], etc. However, to the extent of our knowledge, the denoising of MRI images using CNN has not been extensively studied in the literature. Zhang et al. [25] have developed a deep CNN architecture for denoising of additive gaussian noise. They have shown that deep CNNs are more efficient than traditional methods in terms of the performance and time-complexity both. Further, researchers [26] have designed a fast and flexible denoising CNN (FFDNet) for removal of noise. This method has the ability to handle white gaussian and spatially variant noise. However, their method requires a noise level map for denoising of spatially varying noise. More recently, Jiang et al. [12] have developed a ten layer CNN for MRI denoising. They have adopted VGG network [21] architecture for noise reduction. The residual learning strategy is also employed in this method. The residual learning [10] uses the short-cut connections for faster and effective training of deep CNNs. Motivated by recent advancements in CNN, we have proposed a novel CNN-based MRI denoising method.

The main contributions of the proposed work are listed as follows:

- We have proposed a novel CNN architecture for denoising of MRI scans. The proposed architecture utilizes the encoder-decoder structure.
- The residual learning strategy is exploited in the proposed method. The local as well as global residual learning are applied in the proposed denoising framework. The local residual learning helps to boost the training process, whereas the global residual learning helps to retain prominent image features.
- The training dataset has been prepared with simulated brain MRI images. We have synthetically added rician noise in the training images. The testing of the network has been carried out on synthetic and real MRI images.
- For experimental analysis, we have collected an MRI dataset from a hospital in our locality. Additionally, we have considered four more benchmark datasets for the result analysis.

The rest of the letter has been categorized as follows: Section 2 describes the proposed MRI denoising network, the experimental results have been presented in Section 3, and concluding remarks have been discussed in Section 4.

2. The proposed MRI denoising network

In this section, we have introduced the proposed CNN-based MRI denoising framework. The proposed network attempts to learn prior image features from the image domain in order to map a noise-free image from its noisy counterpart. The following subsections provide detail discussion on CNN-DMRI in terms of overall architecture design, main building blocks, salient features, and loss function.

2.1. Network architecture design

As depicted in Fig. 1, the proposed denoising network takes a noisy MRI as an input and outputs its clear version. It is actually a generative network, which utilizes the encoder-decoder framework. The network performs down-sampling and up-sampling with a scale factor of 2. The first two layers of the network comprise two convolution (CONV) layers, which includes 64 filters of sizes 3×3. Followed by initial CONV layers, the architecture contains two-step down-sampling of the image. These layers encodes an input of size $256 \times 256 \times 64$ to $64 \times 64 \times 128$ tensor. The encoded features are then fed into a set of residual blocks. Each residual block contains a skip connection, which allows local residual learning. These blocks attempt to extract deep features that are required for denoising. To decode the output of the previous layers, the network performs two de-convolutions that up-sample the output of the residual blocks to $256 \times 256 \times 64$. The output of the up-sampling layers is then fed into a convolution layer, which is finally added with input MRI image to obtain the clean MRI. The network consists of total 1,627,009 parameters.

2.2. Encoder-decoder structure

The proposed denoising network incorporates popular encoder-decoder structure. It is built up using three components, namely encoder, residual units, and decoder. The encoder performs some transformations on input tensor and then it down-sizes the tensor. The residual units extract useful deep features for denoising. Based on the extracted features, the decoder produces an approximation of the target image by performing up-sampling and few transformations. This process particularly helps to preserve critical image features and ignore useless ones. Due to this, the network achieves better generalization ability than a simple CNN.

2.3. Residual learning

The residual learning is utilized in the proposed denoising network for faster and effective training [10]. The network applies residual learning on two levels, namely local and global. The local residual learning is incorporated in the middle of the network or just after the down-sampling process. Four residual blocks are used in the middle of the network, which performs local residual learning. Each residual block contains a skip-connection in it. The configuration of a residual block used in the proposed network is depicted in Fig. 2. In this figure, CONV, ReLU, and BN represent convolution, rectified linear unit, and batch normalization, respectively. The size of the convolution is 3×3, and it contains 128 filters. The batch normalization (BN), added in these layers, helps to diminish the effect of internal covariate shift and thereby boosts the training process.

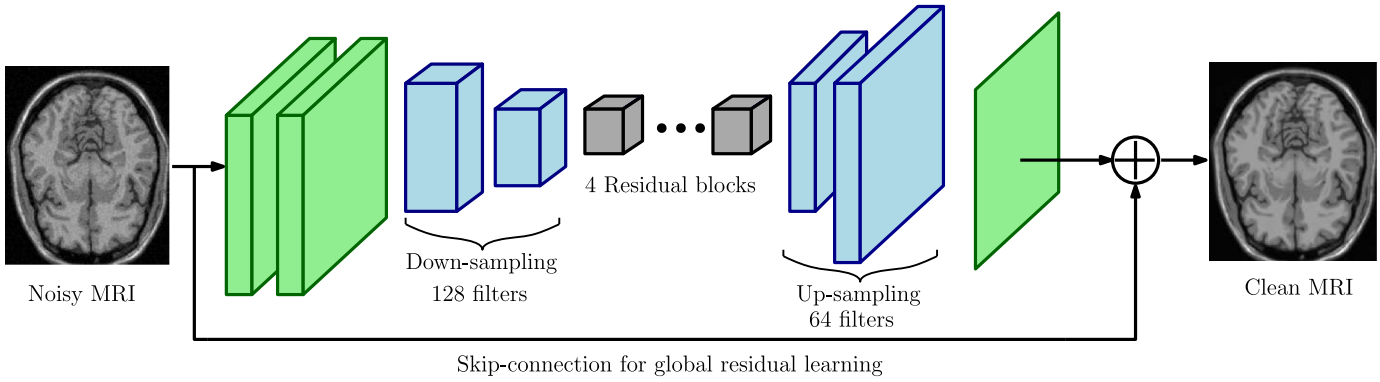

Fig. 1. The architecture of proposed MRI denoising network. The brain MRI images shown here are taken from Brainweb dataset. Refer Fig. 2 for the configuration of residual blocks.

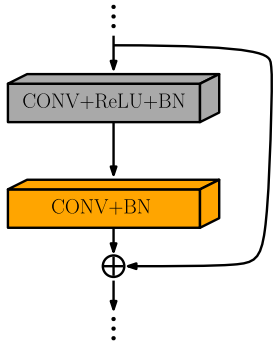

Fig. 2. A residual block used in the middle of proposed CNN-DMRI. Each convolution comprises 128 filters.

The global residual learning is also incorporated in the proposed network. A skip-connection is specifically introduced in the proposed network (see Fig. 1) for utilizing global residual learning. In doing so, the entire architecture works as a single global residual block. This type of scheme helps the network to avoid any potential feature loss during the intermediate stages of denoising.

2.4. Loss function

A loss function plays a crucial role in the training of a neural network. The choice of a loss function typically depends on the problem to be solved. For image restoration and image super resolution tasks [15,25], Mean Squared Error (MSE) has been quite successful. So, we have taken MSE as a loss function for the proposed CNN-DMRI. Given X is a true MRI and Y is its noisy counterpart, MSE is defined as follows.

$$MSE = \frac{1}{P \times Q} \sum_{i=1}^{P} \sum_{j=1}^{Q} ||X(i,j) - \phi(Y(i,j))||_2^2, \tag{3}$$

where ϕ denotes a trained model or parameters through which the estimated MRI image $\hat{X}$ can be generated. It may be noted that the sizes of X and Y are $P \times Q$.

3. Experimental results and analysis

We have tested the performance of the proposed denoising network on simulated and real MRI scans. In this section, we discuss dataset description, training of the network, results analysis, and comparative study.

3.1. Dataset description

The performance of the proposed network has been assessed on five MRI datasets. The first dataset contains simulated brain MRI images which are acquired from Brainweb [5]. The dataset comprises T1-w MRI images that have a resolution of 217 × 181. The second dataset used for results analysis is IXI dataset [11]. This dataset consists of real brain MRI images that were acquired from two hospitals, namely Hammersmith and Guys hospital. The brain images from the first hospital were produced with Philips 3 Tesla MRI workstation, whereas the images of the second hospital were taken with Philips 1.5 Tesla MRI machine. The MRI slices in this dataset are of resolution 256 × 256. We have used Multiple Sclerosis (MS) dataset [16] by University of Syprus as a third dataset. This dataset comprises T2-w MRI images which have resolution of 256 × 256. We have also included a Prostate MRI dataset [20] for the result analysis. The prostate MRI scans in this fourth dataset have the resolution of 256 × 256. The fifth dataset used in this work is collected by us from Asian Dwaraka Jalan hospital, Dhanbad. The dataset consists of MRI brain slices of size 204 × 256. It consists of 51 brain MRI scans of different subjects. These MRI scans have been produced with Siemens 1.5 Tesla MRI workstation.

3.2. Training of the network

Training of a deep neural network usually requires a huge amount of supervised data. However, it is not feasible to prepare such data for MRI denoising task. To solve this issue, we have specifically trained our network on synthetic MRI images. We have taken 100 T1-w brain MRI images from Brainweb dataset. The images have been partitioned into three sets as training, validation, and testing set. The training set contains 65 images, whereas validation and testing set comprises 15 images each. In these sets, we have synthetically added rician noise in the range [1, 30]. After adding noise, the training, validation, and test set have 1950, 450, and 450 MRI images, respectively. The proposed denoising network has been trained on this dataset in an end-to-end way by optimizing the loss function given in Eq. (3).

We have used Adaptive moment estimation (Adam) [13] as a learning scheme. The initial learning rate is set to 0.001 and it is reduced by factors of 0.5, 0.25, and 0.125 in the next three quarters. The training is conducted for 25 epochs. Fig. 3 depicts the performance of the network in terms of peak signal to noise ratio (PSNR) over different epochs on the validation set. The batch size for the training is chosen as 8, which balances the trade-off between GPU memory and training speed. The proposed denoising CNN has been implemented in Python with Tensorflow support.

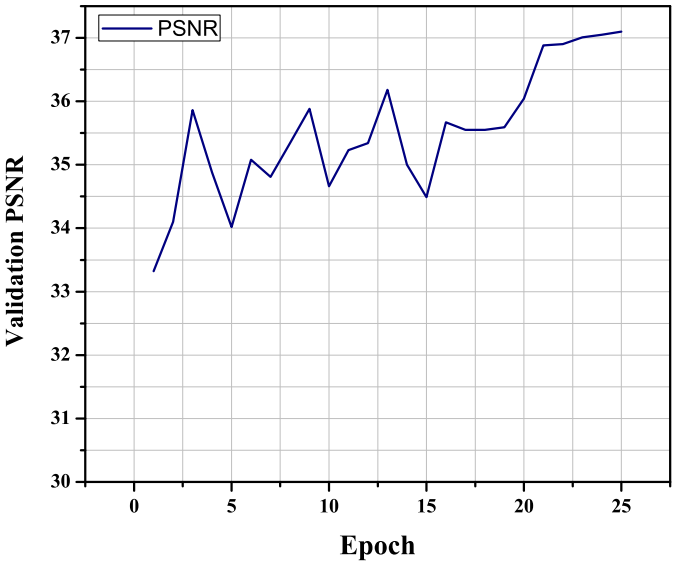

Fig. 3. PSNR on the validation set during different epochs of the training.

The training of the network is performed using NVIDIA Tesla K-80 GPU.

3.3. Results analysis

The performance of the proposed method has been tested through quantitative and qualitative results. For quantitative results analysis, we have used two popular performance measures, namely peak signal to noise ratio (PSNR) and structural similarity index (SSIM). PSNR and SSIM are estimated as follows.

$$PSNR = 10\log_{10}\left(\frac{255^2}{MSE}\right), \tag{4}$$

where MSE denotes mean squared error between real or noise-free image and denoised image,

$$SSIM = \frac{(2\mu_X\mu_{\hat{X}} + t_1)(2\sigma_{X\hat{X}} + t_2)}{(\mu_X^2 + \mu_{\hat{X}}^2 + t_2)(\sigma_X^2 + \sigma_{\hat{X}}^2 + t_2)}, \tag{5}$$

where μ_X and $\mu_{\hat{X}}$ are means of noisy-free image and denoised image; t_1 and t_2 are constants; σ_X^2 and $\sigma_{\hat{X}}^2$ represent the variances; $\sigma_{X\hat{X}}$ shows the covariance between X and $\hat{X}$.

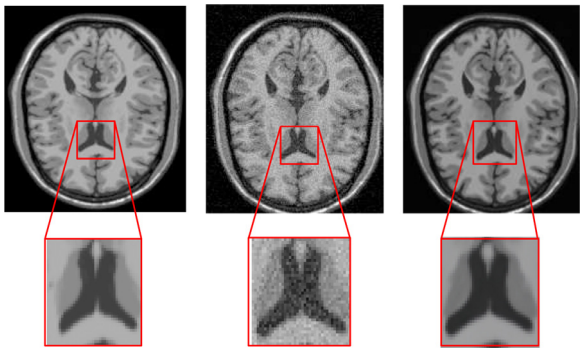

Fig. 5. Denoising of a brain MRI of Brainweb dataset. First column: Clean MRI scan, Second column: MRI corrupted with 13% noise, Third column: Denoised MRI.

The qualitative denoising results for different brain MRI images are depicted in Fig. 4. In this figure, the results are presented in a row-wise fashion, where the first row shows clean MRI scans of five datasets. The images in the second row are contaminated with 9% rician noise, whereas the third row illustrates the denoising outcomes of our method for each image. From these results, it can be observed that the denoising results are very similar to the clean MRI images and the denoised images do not have any noticeable artefact. Furthermore, denoising result for a brain slice of Brainweb dataset is shown in Fig. 5. The second image in this figure is corrupted with 13% rician noise. In the marked area, we can notice that the structure of ventricle in the denoised image (i.e., third image) is well preserved. This indicates that our method not only reduces the noise effectively but also retains the structural detail in MRI images.

We have also used our CNN to denoise a set of real MRI images which have pre-existing noise. Fig. 6 depicts the denoising outcomes of few of sample images. These MRI scans are contaminated with very high noise. From this figure, we can notice that the denoising results are very effective. If we see the marked regions in the first and the second image, we can observe that the structure of ventricles is retained effectively in denoised MRI images. The third and fourth image contain a brain tumor. The boundary of the tumor is very vague in the noisy images. However, after denoising of these images, the boundary of the tumor becomes very clear as shown in the marked regions.

Next, we have presented the quantitative denoising results in terms of PSNR and SSIM in Table 1. The table reports the results for

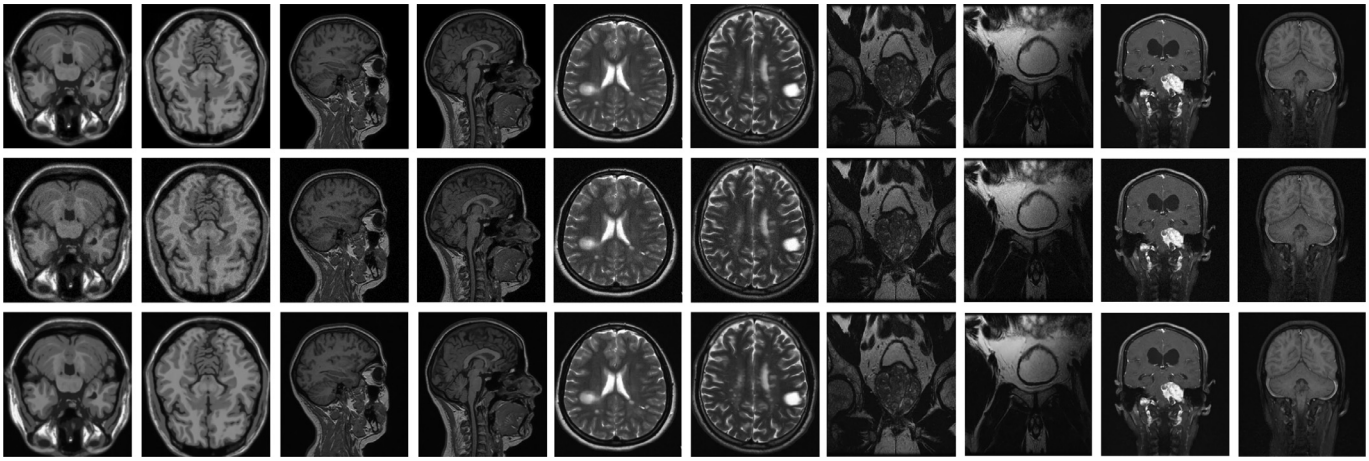

Fig. 4. MRI denoising results on five datasets. First row: clean MRI scans, Second row: MRI scans corrupted with 9% noise, Third row: denoised images. First two images (i.e.,Column 1–2) are taken from Brainweb dataset, next two images (i.e.,Column 3–4) are taken from IXI dataset, next two images (i.e.,Column 5–6) are taken from MS dataset, next two images (i.e.,Column 7–8) are taken from Prostate dataset, and last two images (i.e.,Column 9–10) are taken from our dataset.

Table 1
The quantitative denoising results of our method on different noise levels for five different datasets.

Dataset	Metric	Noise Levels														
		1%	3%	5%	7%	9%	11%	13%	15%	17%	19%	21%	23%	25%	27%	29%
Brainweb	PSNR	40.31	39.55	38.73	38.11	37.55	37.01	36.49	36.04	35.59	35.16	34.71	34.29	33.83	33.46	33.02
	SSIM	0.834	0.827	0.821	0.818	0.815	0.815	0.813	0.812	0.810	0.809	0.806	0.802	0.797	0.791	0.785
IXI	PSNR	39.19	38.38	37.40	36.56	35.83	35.18	34.58	34.07	33.60	33.14	32.68	32.35	31.93	31.58	31.24
	SSIM	0.770	0.762	0.750	0.736	0.729	0.720	0.718	0.713	0.707	0.698	0.692	0.692	0.684	0.672	0.663
MS	PSNR	38.87	38.51	37.95	37.27	36.56	35.78	35.09	34.44	33.84	33.31	32.80	32.32	31.89	31.46	31.07
	SSIM	0.972	0.970	0.966	0.961	0.955	0.948	0.942	0.935	0.927	0.920	0.912	0.903	0.895	0.886	0.876
Prostate	PSNR	36.79	36.35	35.67	34.87	34.03	33.24	32.55	31.93	31.43	30.98	30.61	30.28	29.98	29.71	29.45
	SSIM	0.951	0.944	0.933	0.919	0.902	0.885	0.868	0.852	0.837	0.823	0.811	0.799	0.788	0.778	0.768
Our Dataset	PSNR	39.49	38.82	38.02	37.22	36.47	35.77	35.14	34.59	34.17	34.08	33.64	32.87	32.51	32.20	31.89
	SSIM	0.966	0.959	0.950	0.940	0.931	0.921	0.912	0.904	0.901	0.895	0.888	0.872	0.865	0.857	0.850

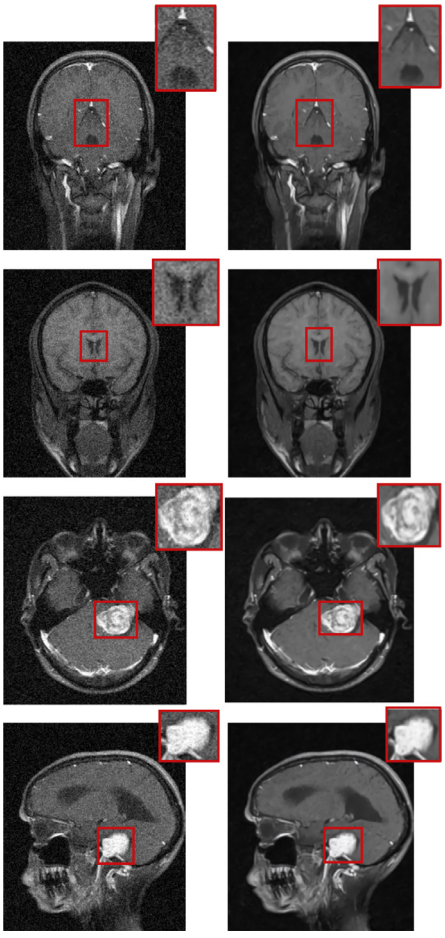

Fig. 6. Denoising of MRI scans with pre-existing noise. First column: MRI scans corrupted with noise and Second column: Denoised MRI scans.

five datasets for different noise levels. The testing noise levels are taken from 1% to 29%. This range has been decided after consulting with different radiologists in our locality. It is suggested that noise range [1, 15] is frequently found in MRI scans taken with 1.5 Tesla scanner. However, the upper limit usually increases if the scans are taken in very shorter times or improper setting of radio-frequency coils. To cover a wide range of noise levels, we have taken testing noise levels from 1% to 29%. From the reported results in Table 1, we can notice that the results for Brainweb dataset are slightly better than the other datasets. This has happened because the training of the network is specifically performed on Brainweb dataset. The other four datasets have been only used for the testing purpose. However, the results for the other datasets are also very impressive, which shows that the proposed denoising network has a nice generalization ability. To show the improvements obtained in denoised images over noisy images, we have compared the PSNR values of noisy and denoised images. Fig. 7 graphically illustrates the improvements achieved in PSNR values on different datasets. We can notice from these graphs that the improvements are very significant for noise levels greater than 3%.

Table 2
The results of our method when training with noise range [1, 10] and testing with noise range [11, 20].

Dataset	Metric	Noise Levels				
		11%	13%	15%	17%	19%
Brainweb	PSNR	36.23	35.37	34.50	33.69	32.91
	SSIM	0.793	0.783	0.772	0.761	0.750
IXI	PSNR	34.69	33.91	33.18	32.46	31.78
	SSIM	0.706	0.691	0.675	0.660	0.643
MS	PSNR	35.76	34.97	34.18	33.43	32.71
	SSIM	0.942	0.929	0.915	0.900	0.884
Prostate	PSNR	33.21	32.34	31.52	31.08	30.59
	SSIM	0.884	0.858	0.850	0.821	0.815
Our Dataset	PSNR	34.95	34.34	33.78	33.32	32.78
	SSIM	0.906	0.894	0.881	0.870	0.859

We have also performed blind denoising of MRI images by the proposed network. The blind denoising means that the network trained for a particular noise level should not be tested for same noise level. Therefore, we can say that the testing noise level should be unseen for the network. We have taken two cases to handle such types of scenarios. In the first case, the network is trained for noise range [1, 10] and tested for noise range [11, 20] (see Table 2). If we compare the results of Table 1 and 2, we can notice that the performance of the network is reduced in Table 2. In the second case, we have trained the network for noise range [11, 20] and tested for noise range [1, 10] (see Table 3). Again if we compare the results of Tables 1 and 3, we can notice that the performance of network is improved in Table 3. With these results, we can conclude that the performance of the network, trained with high noise levels and tested with low noise levels, is higher than

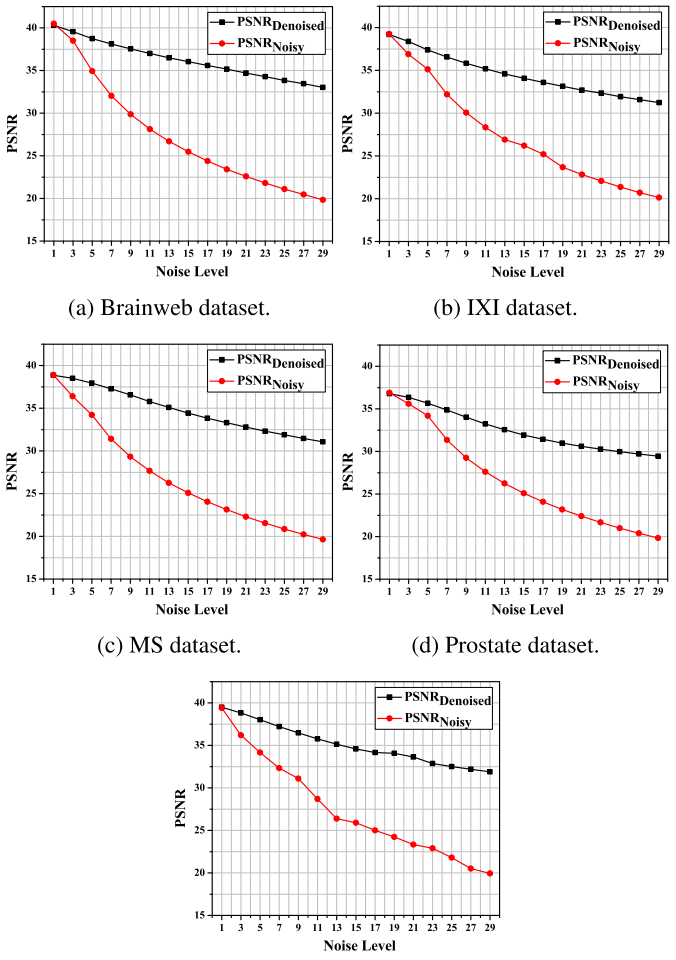

(a) Brainweb dataset. (b) IXI dataset.

(c) MS dataset. (d) Prostate dataset.

(e) Our dataset.

Fig. 7. PSNR comparison between noisy images and denoised images for different datasets.

Table 3
The results of our method when training with noise range [11, 20] and testing with noise range [1, 10].

Dataset	Metric	Noise Levels				
		1%	3%	5%	7%	9%
Brainweb	PSNR	43.18	42.72	42.02	41.11	40.19
	SSIM	0.987	0.987	0.987	0.985	0.982
IXI	PSNR	39.30	39.02	38.52	37.88	37.19
	SSIM	0.977	0.976	0.972	0.966	0.959
MS	PSNR	42.22	41.24	39.92	38.54	37.34
	SSIM	0.980	0.976	0.971	0.964	0.956
Prostate	PSNR	41.37	39.89	37.95	36.21	34.90
	SSIM	0.977	0.968	0.953	0.934	0.915
Our Dataset	PSNR	40.84	40.37	39.38	38.11	37.04
	SSIM	0.975	0.968	0.958	0.945	0.932

the network trained and tested with same noise levels. However, the opposite case is not true.

3.4. Comparative analysis with existing methods

The performance of the proposed denoising network has also been compared with some existing works [6,7,12,18,26]. Table 4 provides a comparative analysis of different methods on the basis of PSNR. The different methods are compared on seven types of noise levels (i.e., 3%, 5%, 7%, 9%, 11%, 13%, and 15%). This table contains two types of comparing methods. The methods such as FFD-Net [26] and MCDnCNNg [12] are CNN-based methods, whereas the methods such as NLM [6], PRI-NL-PCA [18], and CNLM [7] are non-CNN-based methods. In order to perform unbiased comparison of the results, we have used the same training data for CNN-based methods. In non-CNN-based methods, we have used search window and similarity window of sizes 7×7 and 3×3, respectively. From the reported results in Table 4, one can observe that our CNN-DMRI has produced highly competitive results. In fact, it has outperformed for noise levels 5%, 7%, 9%, 11%, 13%, and 15% for all datasets.

Finally, we have analyzed the computation time of different methods. We have estimated the average computation time (in seconds) of all testing images. CNN-based methods enjoy faster denoising due to the utilization of GPU computation. We have used NVIDIA Tesla K-80 GPU for CNN-based methods. Our CNN-DMRI has taken 0.32 seconds, whereas MCDnCNNg and FFDNet have taken 0.48 and 0.29 seconds respectively for denoising of an MRI scan. We have utilized CuDNN library for accelerating GPU computation. The multi-threaded implementation of CNLM has taken 45.7 seconds on intel core i5 processor, whereas NLM and PRI-NL-PCA have consumed 43.1 and 41.8 seconds respectively for denoising of an MRI. Though FFDNet is slightly faster than our CNN, by considering the improvements in denosing results, the proposed denoising network can be a favorable choice for MRI denoising.

Table 4
Comparative study with different methods in terms of PSNR on five dataset. Best values are given in bold.

Dataset	Methods	Noise Levels						
		3%	5%	7%	9%	11%	13%	15%
Brainweb	NLM	32.53	31.19	30.09	29.17	28.80	28.24	27.89
	PRI-NL-PCA	39.34	36.58	34.74	33.28	32.16	31.41	30.21
	CNLM	37.18	33.88	33.01	31.58	31.16	30.71	30.13
	FFD-Net	39.11	36.34	34.87	33.91	33.26	32.59	32.11
	MCDnCNNg	38.10	36.00	34.50	33.00	32.53	32.20	32.01
	CNN-DMRI	**39.55**	**38.73**	**38.11**	**37.55**	**37.01**	**36.49**	**36.04**
IXI	NLM	33.42	32.98	32.31	31.77	31.21	30.14	29.32
	PRI-NL-PCA	38.54	36.21	34.34	33.58	32.36	32.01	31.21
	CNLM	37.02	33.47	32.61	32.11	31.46	30.61	29.70
	FFD-Net	38.74	36.88	36.49	34.85	33.66	33.01	32.01
	MCDnCNNg	**39.38**	37.12	35.40	33.86	32.54	31.10	29.96
	CNN-DMRI	38.38	**37.40**	**36.56**	**35.83**	**35.18**	**34.58**	**34.07**
MS	NLM	33.57	32.47	31.98	31.39	31.08	30.31	29.56
	PRI-NL-PCA	38.39	37.28	36.84	33.18	32.40	31.87	31.07
	CNLM	37.08	34.12	33.41	32.79	32.06	31.62	30.48
	FFD-Net	38.47	37.78	36.87	34.89	33.96	32.81	32.43
	MCDnCNNg	**38.84**	37.32	36.98	34.71	33.74	32.90	31.94
	CNN-DMRI	38.51	**37.95**	**37.27**	**36.56**	**35.78**	**35.09**	**34.44**
Prostate	NLM	32.38	31.90	30.19	29.87	29.40	28.94	28.09
	PRI-NL-PCA	36.11	35.38	34.24	33.27	32.46	32.02	31.09
	CNLM	35.21	34.09	33.32	32.14	31.78	30.97	30.14
	FFD-Net	36.21	35.28	34.56	33.85	33.06	32.38	31.31
	MCDnCNNg	36.26	35.12	34.49	33.80	33.12	32.41	31.62
	CNN-DMRI	**36.35**	**35.67**	**34.87**	**34.03**	**33.24**	**32.55**	**31.93**
Our dataset	NLM	32.11	31.62	31.02	30.87	30.06	29.17	28.81
	PRI-NL-PCA	37.84	36.79	35.86	35.08	34.17	33.10	32.31
	CNLM	35.32	34.09	33.12	32.49	31.87	30.98	30.03
	FFD-Net	**38.85**	37.84	36.38	35.78	34.70	33.37	32.87
	MCDnCNNg	38.79	37.41	36.94	35.39	34.48	33.23	32.76
	CNN-DMRI	38.82	**38.02**	**37.22**	**36.47**	**35.77**	**35.14**	**34.59**

4. Conclusion

In this letter, we have proposed a new CNN model, namely CNN-DMRI, for reduction of rician noise from MRI images. The proposed CNN consists of multiple convolutions which capture different image features while separating inherent noise. In addition, the proposed method performs down-sampling and up-sampling of images in the denoising process through the encoder-decoder framework. The residual learning is also introduced in the proposed CNN model. The training of the network is carried out with synthetic MRI images. For testing of the results, five datasets have been acquired. Several experiments, conducted on simulated and real MRI scans, indicate that the proposed method achieves promising qualitative and quantitative denoising results. Additionally, the performance of the network has also been analyzed on unseen or blind noise levels. The comparative study has demonstrated that the proposed CNN has performed superior to existing methods.

Declaration of Competing Interest

None.

Acknowledgments

The authors would like to acknowledge Asian Dwaraka Jalan Hospital, Dhanbad for providing MRI dataset.

References

[1] C.S. Anand, J. Sahambi, MRI denoising using bilateral filter in redundant wavelet domain, in: IEEE TENCON, 2008, pp. 1–6.
[2] C.S. Anand, J.S. Sahambi, Wavelet domain non-linear filtering for MRI denoising, Magn. Reson. Imaging 28 (6) (2010) 842–861.
[3] F. Baselice, G. Ferraioli, V. Pascazio, A. Sorriso, Denoising of MR images using kolmogorov-smirnov distance in a non local framework, Magn. Reso.n Imaging 57 (2019) 176–193.
[4] H.V. Bhujle, B.H. Vadavadagi, NLM Based magnetic resonance image denoising–a review, Biomed. Signal. Process Control 47 (2019) 252–261.
[5] Brainweb, Simulated brain database, McConnell Brain Imaging Centre, Montreal Neurological Institute, McGill, 2004. http://brainweb.bic.mni.mcgill.ca/brainweb
[6] A. Buades, B. Coll, J.-M. Morel, A non-local algorithm for image denoising, in: IEEE Conference on Computer Vision and Pattern Recognition, 2, 2005, pp. 60–65.
[7] G. Chen, P. Zhang, Y. Wu, D. Shen, P.-T. Yap, Denoising magnetic resonance images using collaborative non-local means, Neurocomputing 177 (2016) 215–227.
[8] G. Gerig, O. Kubler, R. Kikinis, F.A. Jolesz, Nonlinear anisotropic filtering of MRI data, IEEE Trans. Med. Imaging 11 (2) (1992) 221–232.
[9] S. Gu, L. Zhang, W. Zuo, X. Feng, Weighted nuclear norm minimization with application to image denoising, in: IEEE Conference on Computer Vision and Pattern Recognition, 2014, pp. 2862–2869.
[10] K. He, X. Zhang, S. Ren, J. Sun, Deep residual learning for image recognition, in: Proceedings of the IEEE Conference on Computer Vision and Pattern Recognition, 2016, pp. 770–778.
[11] IXI MRI, Brain MRI database, Imperial College London (2018). https://brain-development.org/ixi-dataset
[12] D. Jiang, W. Dou, L. Vosters, X. Xu, Y. Sun, T. Tan, Denoising of 3D magnetic resonance images with multi-channel residual learning of convolutional neural network, Jpn. J. Radiol. 36 (9) (2018) 566–574.
[13] D.P. Kingma, J. Ba, Adam: a method for stochastic optimization, arXiv Preprint arXiv:1412.6980 (2014).
[14] K. Krissian, S. Aja-Fernández, Noise-driven anisotropic diffusion filtering of MRI, IEEE Trans. Image Process. 18 (10) (2009) 2265–2274.
[15] G. Lin, Q. Wu, L. Qiu, X. Huang, Image super-resolution using a dilated convolutional neural network, Neurocomputing 275 (2018) 1219–1230.
[16] C.P. Loizou, V. Murray, M.S. Pattichis, I. Seimenis, M. Pantziaris, C.S. Pattichis, Multiscale amplitude-modulation frequency-modulation (am–fm) texture analysis of multiple sclerosis in brain mri images, IEEE Trans. Inf. Technol. Biomed. 15 (1) (2010) 119–129.
[17] J.V. Manjón, J. Carbonell-Caballero, J.J. Lull, G. García-Martí, L. Martí-Bonmatí, M. Robles, MRI Denoising using non-local means, Med. Image Anal. 12 (4) (2008) 514–523.
[18] J.V. Manjón, P. Coupé, A. Buades, MRI Noise estimation and denoising using non-local PCA, Med. Image Anal. 22 (1) (2015) 35–47.
[19] R.D. Nowak, Wavelet-based rician noise removal for magnetic resonance imaging, IEEE Trans. Image Process. 8 (10) (1999) 1408–1419.
[20] Prostate MRI, Prostate MR image database, National Center for Image Guided Therapy (2008). https://http://prostatemrimagedatabase.com
[21] K. Simonyan, A. Zisserman, Very deep convolutional networks for large-scale image recognition, arXiv preprint arXiv:1409.1556 (2014).
[22] J. Tang, Q. Sun, J. Liu, Y. Cao, An adaptive anisotropic diffusion filter for noise reduction in MR images, in: International Conference on Mechatronics and Automation, 2007, pp. 1299–1304.
[23] P. Wang, H. Zhang, V.M. Patel, SAR Image despeckling using a convolutional neural network, IEEE Signal Process. Lett. 24 (12) (2017) 1763–1767.
[24] A.M. Wink, J.B. Roerdink, Denoising functional MR images: a comparison of wavelet denoising and gaussian smoothing, IEEE Trans. Med. Imaging 23 (3) (2004) 374–387.
[25] K. Zhang, W. Zuo, Y. Chen, D. Meng, L. Zhang, Beyond a gaussian denoiser: residual learning of deep CNN for image denoising, IEEE Trans. Image Process. 26 (7) (2017) 3142–3155.
[26] K. Zhang, W. Zuo, L. Zhang, FFDNet: Toward a fast and flexible solution for cnn-based image denoising, IEEE Trans. Image Process. 27 (9) (2018) 4608–4622.